Check for updates

AGU ADVANCING EARTH AND SPACE SCIENCES

AGU Advances

RESEARCH ARTICLE
10.1029/2025AV002040

No "Wet Gets Wetter" in Kilometer-Scale Mock-Walker Circulations

Adam B. Sokol[1], **Timothy M. Merlis**[1], **and Stephan Fueglistaler**[1]

[1]Program in Atmospheric and Oceanic Sciences, Princeton University, Princeton, NJ, USA

Peer Review The peer review history for this article is available as a PDF in the Supporting Information.

Key Points:

- Mock-Walker simulations with varied ocean boundary conditions show a wet-gets-drier response to warming and ascent region expansion
- Expansion occurs because moisture transport by the weakening atmospheric circulation does not keep pace with increasing precipitation
- Circulation weakening is driven by increasing gross moist stability related to changes in circulation vertical structure

Supporting Information:

Supporting Information may be found in the online version of this article.

Correspondence to:

A. B. Sokol,
adam.sokol@princeton.edu

Citation:

Sokol, A. B., Merlis, T. M., & Fueglistaler, S. (2026). No "wet gets wetter" in kilometer-scale mock-Walker circulations. *AGU Advances*, *7*, e2025AV002040. https://doi.org/10.1029/2025AV002040

Received 2 SEP 2025
Accepted 5 FEB 2026

Author Contributions:

Conceptualization: Adam B. Sokol
Formal analysis: Adam B. Sokol
Funding acquisition: Timothy M. Merlis, Stephan Fueglistaler
Investigation: Adam B. Sokol
Methodology: Adam B. Sokol
Project administration: Timothy M. Merlis, Stephan Fueglistaler
Software: Adam B. Sokol
Supervision: Timothy M. Merlis, Stephan Fueglistaler
Visualization: Adam B. Sokol
Writing – original draft: Adam B. Sokol

© 2026. The Author(s).
This is an open access article under the terms of the Creative Commons Attribution-NonCommercial License, which permits use, distribution and reproduction in any medium, provided the original work is properly cited and is not used for commercial purposes.

Abstract Many climate model simulations and limited observations indicate that regions of tropical ascent and precipitation contract in response to surface warming. This response has well-studied implications for the width of the zonal- and annual-mean Intertropical Convergence Zone, but its applicability to zonally asymmetric circulations such as the Pacific Walker circulation remains unknown. Here, we investigate the impact of warming on the area of large-scale ascent in kilometer-scale, mock-Walker simulations with both fixed and interactive surface temperatures. Contrary to the "wet-gets-wetter" and "upped-ante" paradigms of precipitation change, the simulations show a "wet-gets-drier" response to warming in which the ascent region becomes larger and, on average, drier. We attribute these changes to rapid circulation weakening, which limits the transport of moisture into the ascent region. To meet the growing moisture demand for precipitation, local evaporation within the ascent region must increase rapidly, and the ascent region expands to draw moisture from a larger surface area. We link the slowdown of the circulation to increases in gross moist stability driven by a previously unknown mechanism. Central to this mechanism are changes in the vertical structure of the circulation, which features two vertically stacked overturning cells reminiscent of some tropical convergence zones. These results challenge long-held paradigms of tropical precipitation change and show that the vertical structure of tropical circulations can play a critical role in the hydrological response to warming.

Plain Language Summary An important goal of climate science is to understand how changes in Earth's surface temperature impact the spatial distribution of rainfall. On very large scales, the precipitation response to warming is sometimes summarized as "wet gets wetter, dry gets drier." This wet-gets-wetter response, along with another hypothesis called the "upped-ante" mechanism, suggest that regions of tropical rainfall contract and intensify with warming. Ample evidence supports this response for the case of the annual-mean Hadley circulation, in which moist air ascends near the equator and descends in the subtropics. We test whether this response also applies to east-west overturning circulations like the Pacific Walker circulation, in which air ascends in the western tropical Pacific and descends in the Eastern Pacific. Surprisingly, in our idealized simulations of the Walker circulation, we find the opposite response: rainy regions expand as the surface warms, and the mean rainfall within them decreases, that is, a "wet-gets-drier" response. We show that this response is driven by a rapid slowdown of the Walker circulation with warming, which we tie to changes in the vertical structure of the circulation.

1. Introduction

Tropical circulations such as the Hadley and Walker circulations consist of distinct regions of dry subsidence and moist, rainy ascent. These two regimes have starkly different hydrological, radiative, and dynamical properties, and changes in their relative area would have significant impacts on water and energy budgets at both regional and global scales (Pierrehumbert, 1995; Su et al., 2020). Accordingly, understanding the impact of warming on ascent fraction—defined here as the portion of the tropics with mean ascent—is a high priority within tropical climatology.

The hydrological response to warming is shaped by dynamic and thermodynamic influences. As the troposphere warms, its moisture content increases by ~7%/K following Clausius-Clapeyron scaling. This leads to commensurate increases in moisture convergence in the tropical rain belts, if the atmospheric circulation is fixed (Held & Soden, 2006). But the tropical circulation is expected to weaken with warming (Knutson & Manabe, 1995; Vecchi & Soden, 2007), counteracting thermodynamically driven increases in moisture convergence. The total precipitation change depends on the relative strengths of these thermodynamic and dynamic factors, which vary

Writing – review & editing: Adam B. Sokol, Timothy M. Merlis, Stephan Fueglistaler

regionally and between different models (Chadwick et al., 2013; Elbaum et al., 2022; Ma et al., 2018; Seager et al., 2010). Held and Soden (2006) found that model-predicted changes in *zonal-mean* moisture convergence are well captured by thermodynamic changes alone; that is, changes in zonal-mean circulation strength were small compared to Clausius-Clapeyron increases in water vapor, so the existing pattern of moisture convergence is simply amplified. This response, which became known as the "wet gets wetter, dry gets drier" pattern, does not imply any change in ascent fraction or the area of significant precipitation.

Adding complexity to the wet-gets-wetter response, other proposed mechanisms suggest that regions of tropical ascent contract with warming. In the "upped ante" mechanism proposed by Neelin et al. (2003), this occurs because a warmer troposphere "ups the ante" for convective instability. In core regions of tropical rainfall, convective activity is maintained in warmer climates by increases in low-level moisture. However, at the rainy-region margins, inflow from cooler subsidence regions is unable to meet the higher threshold for convective instability, and convection is suppressed as a result. Describing the same phenomenon from a different perspective, Y. Zhang and Fueglistaler (2019) added that the upped ante for convective instability occurs in coupled general circulation models (GCMs) because the tropical temperature profile is set by the low-level moist static energy (MSE) in convective regions, which are typically found over the warmest surface temperatures. Because warming is fairly uniform in coupled GCMs, and since saturation vapor pressure depends exponentially on temperature, warming broadens the distribution of low-level MSE, barring large changes in relative humidity. Moderately warm regions that could previously support deep convection become increasingly deficient in MSE relative to the warmest regions, and convection is suppressed. As a result, precipitation is increasingly concentrated in the warmest regions. Both of these mechanisms, which are fundamentally thermodynamic and do not account for changes in the tropical circulation, suggest that regions of ascent become smaller and wetter in a warmer world.

In the context of the zonal-mean, annual-mean Hadley circulation, reductions in ascent fraction with warming manifest as a narrowing and wetting of the Intertropical Convergence Zone (ITCZ), sometimes referred to as the "deep tropical squeeze" (Lau & Kim, 2015). This response is supported by observations and models of varying complexity (Ahmed et al., 2023; Byrne & Schneider, 2016; Byrne et al., 2018; Lau & Tao, 2020; Su et al., 2020; Wodzicki & Rapp, 2016), although it is important to note that the seasonal ITCZs widen in some regions in simulations of future warming (Zhou et al., 2020). Compared to the ITCZ, changes in ascent fraction associated with the Pacific Walker circulation are not well understood, and it is unclear whether something akin to the "deep tropical squeeze" would occur in that case as well. Both the Hadley and Walker circulations are expected to weaken with warming, but models and reanalysis suggest that they weaken at different rates (Schwendike et al., 2015; Vecchi & Soden, 2007). This calls into question the assumption made in previous work that changes in circulation strength are small relative to Clausius-Clapeyron scaling. As we will show, this assumption does not hold in the simulations presented here, with important implications for hydrological change.

This paper builds on a handful of previous studies focused on ascent fraction changes in models of the Walker circulation. Contrary to our results, earlier simulations with intermediate-complexity models have shown decreases in ascent fraction with warming (Bretherton et al., 2006; Peters & Bretherton, 2005). Idealized, cloud-resolving simulations by Bretherton et al. (2006) showed a large ∼40% decrease in rainy region width in response to 2 K warming, but changes beyond that single perturbation were not explored. Building on that work, we find a general *increase* in ascent fraction with warming across a larger range of mean climates. However, because the ascent fraction trends are non-monotonic in some cases, our results are not necessarily at odds with the single perturbation experiment in Bretherton et al. (2006).

In Section 2, we describe the set of 36 cloud-resolving, mock-Walker simulations with varied mean climates and sea surface boundary configurations, both fixed and interactive. In Section 3, we show that ascent fraction increases with warming and is associated with a wet-gets-*drier* precipitation response (Section 3.1). Using moisture budget constraints, we find that these changes result from a significant slowdown of the overturning circulation (Section 3.2), which we trace to increasing gross moist stability and changes in the vertical structure of the circulation (Section 3.4). In Section 3.5, we describe how these simulations depart from the seemingly straightforward thermodynamic predictions of the upped-ante hypothesis. In Section 4, we discuss these surprising results and their implications for tropical hydrological change.

25766044, 2026, 1, Downloaded from https://agupubs.onlinelibrary.wiley.com/doi/10.1029/2025AV002040 by Adam, B Sokol - University Of Washington Lib , Wiley Online Library on [20/02/2026]. See the Terms and Conditions (https://onlinelibrary.wiley.com/terms-and-conditions) on Wiley Online Library for rules of use; OA articles are governed by the applicable Creative Commons License

25776004x, 2026, 1, Downloaded from https://agupubs.onlinelibrary.wiley.com/doi/10.1029/2025AV002040 by Adam, B Sokol - University Of Washington Lib , Wiley Online Library on [20/02/2026]. See the Terms and Conditions (https://onlinelibrary.wiley.com/terms-and-conditions) on Wiley Online Library for rules of use; OA articles are governed by the applicable Creative Commons License

2. Simulations

We conduct simulations with the cloud-resolving System for Atmospheric Modeling (SAM; Khairoutdinov & Randall, 2003) with Rapid Radiative Transfer Model radiation (RRTMG; Clough et al., 2005; Mlawer et al., 1997) and SAM's original single-moment microphysics scheme. The domain is two-dimensional with length $L_x = 9{,}216$ km, a horizontal resolution of 3 km, and 96 vertical levels. Because we seek to mimic the Walker circulation in the equatorial Pacific, where the Coriolis parameter goes to zero, we neglect rotational effects. Insolation is spatially uniform and constant in time with no diurnal cycle, following the RCEMIP protocol (Wing et al., 2018). The domain-average zonal wind is nudged to zero on a two-hour timescale to prevent wind oscillations known to occur in zonally elongated domains (Held et al., 1993). Additional model details are provided in Text S1 in Supporting Information S1.

We test six ocean boundary conditions and six climate states for a total of 36 simulations. In all experiments, the initial surface temperature T_s is set as $T_s(x) = \overline{T}_s - (\delta T_s/2)\cos(2\pi x/L_x)$, where $\overline{T}_s$ is the domain mean an the pattern amplitude $\delta T_s = 4$ K for all but one of the simulation sets. The initial T_s is held fixed for 30 days to allow convection to organize over the warm pool, after which one the following boundary conditions takes over:

- *fixed* T_s: T_s is fixed in time. Two simulation sets are conducted with $\delta T_s = 3$ and 4 K, which we denote fix3 and fix4, respectively.
- *slab*: T_s evolves according to the typical slab-ocean equation

$$c\frac{d}{dt}T_s(x) = N(x), \tag{1}$$

  where c is the slab heat capacity, here corresponding to a depth of 10 m of water, and $N(x) = R_{sfc}(x) - H_L(x) - H_S(x) + S(x)$ is the local surface energy imbalance. R_{sfc} is the net downward radiative flux, H_L the latent heat flux, and H_S the sensible heat flux. We impose an ocean heat source $S(x) = \overline{S} - (\delta S/2)\cos(2\pi x/L_x)$, where δS specifies the amplitude and $\overline{S}$ the mean.

We conduct a single set of slab simulations, denoted slabCO_2, in which we perturb the mean climate by varying the atmospheric CO_2 concentration. We use $\overline{S} = -31.5$ W/m^2 and $\delta S = 70$ W/m^2 to achieve climates comparable to the other simulation sets (see Text S2 and Table S1 in Supporting Information S1 for details).

- *modified slab*: Local T_s varies according to a modified version of Equation 1 that keeps the domain-averaged surface temperature $(\overline{T}_s)$ fixed over time. $N(x)$ in Equation 1 is replaced with the *anomalous* energy imbalance $N'(x) = N(x) - \overline{N}$, and the value of $\overline{S}$ becomes irrelevant because there can be no mean temperature change. Three sets of simulations are conducted with δS of 20, 70, and 100 W/m^2, which we refer to as slab20, slab70, and slab100, respectively. The use of a modified slab eliminates the long equilibration times needed for traditional slab simulations, and the similarity of the results to the slabCO_2 runs suggests minimal interference with the relevant physics.

For the five simulation sets in which $\overline{T}_s$ is fixed in time (all but slabCO_2), we vary $\overline{T}_s$ in 2 K increments from 298 to 308 K. Simulations are integrated for 300 days and the last 150 days are used for analysis. The slabCO_2 runs are integrated for varying amounts of time until equilibrium is reached (Table S1 in Supporting Information S1), and the last 250 days are used for analysis. The CO_2 concentrations are chosen so that the resulting $\overline{T}_s$ values are comparable to the other simulation sets.

As in previous work with cloud-resolving models (e.g., Bretherton et al., 2005), we average all output into mesoscale blocks to reduce noise and aid interpretation. The domain is split into 96 blocks, each with a horizontal dimension of 96 km.

We test the sensitivity of our results to L_x with additional experiments on longer and shorter domains (Text S1, Figure S1 in Supporting Information S1). We also test the sensitivity to 2D geometry by repeating the fix4 and slab70 simulations with an added y dimension of 48 km (Figure S2 in Supporting Information S1). While ascent fraction shows some sensitivity to domain geometry, the general pattern of increasing ascent fraction with warming is not sensitive to these choices.

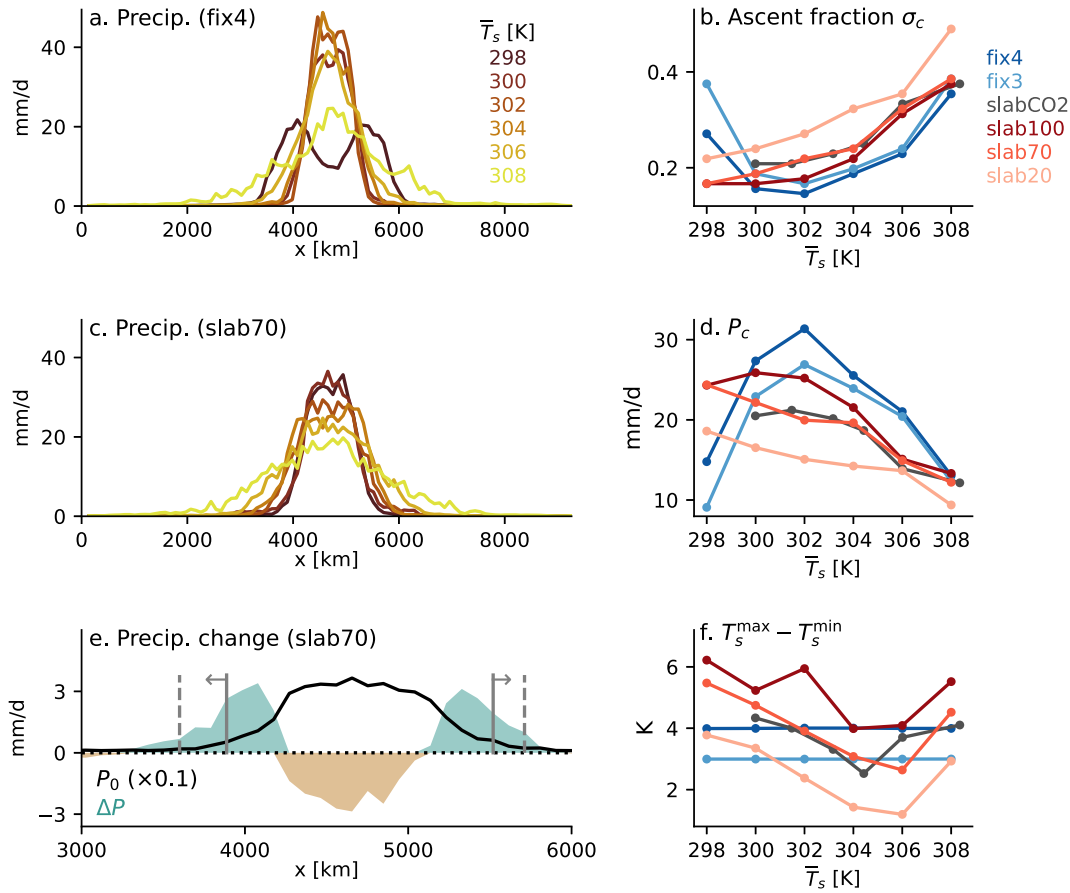

Figure 1. The hydrological response to warming. Precipitation in the (a) fix4 and (c) slab70 simulations (note: the T_s maximum is in the center of the domain). (b) Ascent fraction σ_c. (d) Mean precipitation rate within the ascent region P_c. (e) Precipitation in the 300 K slab70 simulation (black line, scaled by a factor of 0.1) and the change in precipitation between the 300 and 304 K simulations (shading). Solid and dashed gray lines show the ascent region edges for 300 and 304 K, respectively. Note that the x-axis is zoomed in on the center of the domain. (f) Difference between the maximum and minimum block-averaged T_s for each simulation. Panels (a, c, e) are reproduced for the other simulation sets in Figure S3 in Supporting Information S1.

3. Results

3.1. Ascent Region Expansion and the Wet-Gets-Drier Response

We begin by examining changes in precipitation and ascent fraction with warming. We define the ascent fraction σ_c as the fraction of the domain in which the time-averaged tropospheric integral of the vertical velocity is upwards (Equation 2). Throughout the paper, the c subscript denotes a spatial and temporal average over the ascent region. While precipitation is not considered in this definition, regions of mean ascent align very closely with regions of significant rainfall: on average, ∼95% of total precipitation occurs within the ascent region, with the remainder found immediately outside, where there is sporadic convective activity despite mean subsidence.

In all simulations, the rainy region is centered over the warmest T_s in the center of the model domain. Figure 1 shows that the rainy region generally expands with warming due to increases in precipitation at its margins, in direct contradiction of upped-ante expectations. At the same time, the peak precipitation rate, typically found in the center of the rainy region, decreases (Figure 1e). These changes lead to an overall decrease in P_c, the mean precipitation rate within the ascent region (Figure 1d). We refer to this response as a wet-gets-*drier* response, in contrast to the wet-gets-*wetter* response characterizing changes in the zonal-mean, annual-mean Hadley circulation. The wet-gets-drier response, which is seen in all six simulation sets (Figure 1d, Figure S3 in Supporting Information S1), implies that the spatial distribution of rainfall becomes more even with warming.

25766044, 2026, 1, Downloaded from https://agupubs.onlinelibrary.wiley.com/doi/10.1029/2025AV002040 by Adam, B Sokol - University Of Washington Lib , Wiley Online Library on [20/02/2026]. See the Terms and Conditions (https://onlinelibrary.wiley.com/terms-and-conditions) on Wiley Online Library for rules of use; OA articles are governed by the applicable Creative Commons License

2576604x, 2026, 1, Downloaded from https://agupubs.onlinelibrary.wiley.com/doi/10.1029/2025AV002040 by Adam, B Sokol - University Of Washington Lib , Wiley Online Library on [20/02/2026]. See the Terms and Conditions (https://onlinelibrary.wiley.com/terms-and-conditions) on Wiley Online Library for rules of use; OA articles are governed by the applicable Creative Commons License

Commensurate with the precipitation response, σ_c generally increases with warming for all six ocean configurations and in the sensitivity tests with a 3D domain (Figure 1b, Figure S2 in Supporting Information S1). There is notable nonlinearity and, in some cases, non-monotonicity in both the σ_c and P_c response to warming. In the slab simulations, the rate of expansion generally increases with warming. In the fixed-T_s runs, σ_c first decreases between 298 and 302 K before subsequently increasing from 302 to 308 K. We will return to this point in Section 3.4, but for now note that the 298 K fixed-T_s simulations are outliers in that they feature two distinct zones of heavy precipitation within the ascent region (Figure 1a, Figure S3 in Supporting Information S1). The merging of these regions into one produces the initial decrease in σ_c and increase in P_c, after which the wet-gets-drier response takes over.

Previous work predicting a more uneven distribution of rainfall with warming examined scenarios in which the range of tropical T_s within a given climate did not change significantly (Y. Zhang & Fueglistaler, 2019). We must therefore ask whether the surprising trends in σ_c are simply the result of underlying changes in surface temperature gradients, which are known to impact ascent region area (Bretherton & Sobel, 2002). Because T_s sets the moisture content and moist static energy (MSE) of the boundary layer, significant changes in T_s gradients could also interfere with the upped-ante mechanism of ascent region contraction. In line with previous work (Merlis & Schneider, 2011), Figure 1d shows that T_s gradients generally decrease with warming in the slab simulations up to 306 K. Since weaker T_s gradients are associated with larger σ_c (Bretherton & Sobel, 2002), it is possible that the decrease in T_s gradients contributes to ascent region expansion. However, the continued increase in σ_c beyond 306 K despite the reversal of the T_s gradient trend, as well as the increase in σ_c in the fixed-T_s simulations, suggests that T_s gradients are not the primary driver of ascent region expansion. We provide an alternative explanation in the following sections.

3.2. Moisture Budget Interpretation of Ascent Region Expansion

In this section we utilize the moisture budget to show that ascent region expansion is driven by a mismatch between mean precipitation changes and much smaller changes in atmospheric moisture transport (AMT). We first introduce the vertical integration operator $\langle \cdot \rangle$ such that for any variable $\chi(p)$

$$\langle \chi \rangle = \frac{1}{g}\int_{p_t}^{p_s} \chi \, dp \tag{2}$$

where p_t and p_s are the tropopause and surface pressures, respectively. For each simulation, p_T is the level where the domain-averaged streamfunction magnitude reaches zero, indicating the upper extent of the circulation.

We consider the equilibrium moisture budget averaged over the ascent region:

$$P_c - E_c = -\langle \nabla \cdot \overline{uq} \rangle_c. \tag{3}$$

Bars denote temporal averages and the c subscript denotes a spatiotemporal average over the ascent (i.e., convective) region. P is precipitation, E is evaporation, q is specific humidity, and u is the zonal wind. The right-hand side is the AMT term representing moisture convergence into the ascent region by the atmospheric circulation. To bring σ_c into the picture, we can express the right-hand side in terms of the horizontal water vapor flux at the ascent-region boundaries

$$P_c - E_c = \frac{\langle \overline{uq} \rangle_{\text{edge}}}{\sigma_c L_x} \tag{4}$$

where the subscript *edge* denotes the average of the two edges of the ascent region. When calculating u_{edge}, we flip the sign of u on the eastern boundary such that positive u_{edge} always corresponds to flow into the ascent region from the subsiding region. The term $\sigma_c L_x$ is the width of the ascent region.

The mean precipitation rate within the ascent region, P_c, is related to the domain-averaged precipitation by

$$\sigma_c P_c = \alpha [P] \tag{5}$$

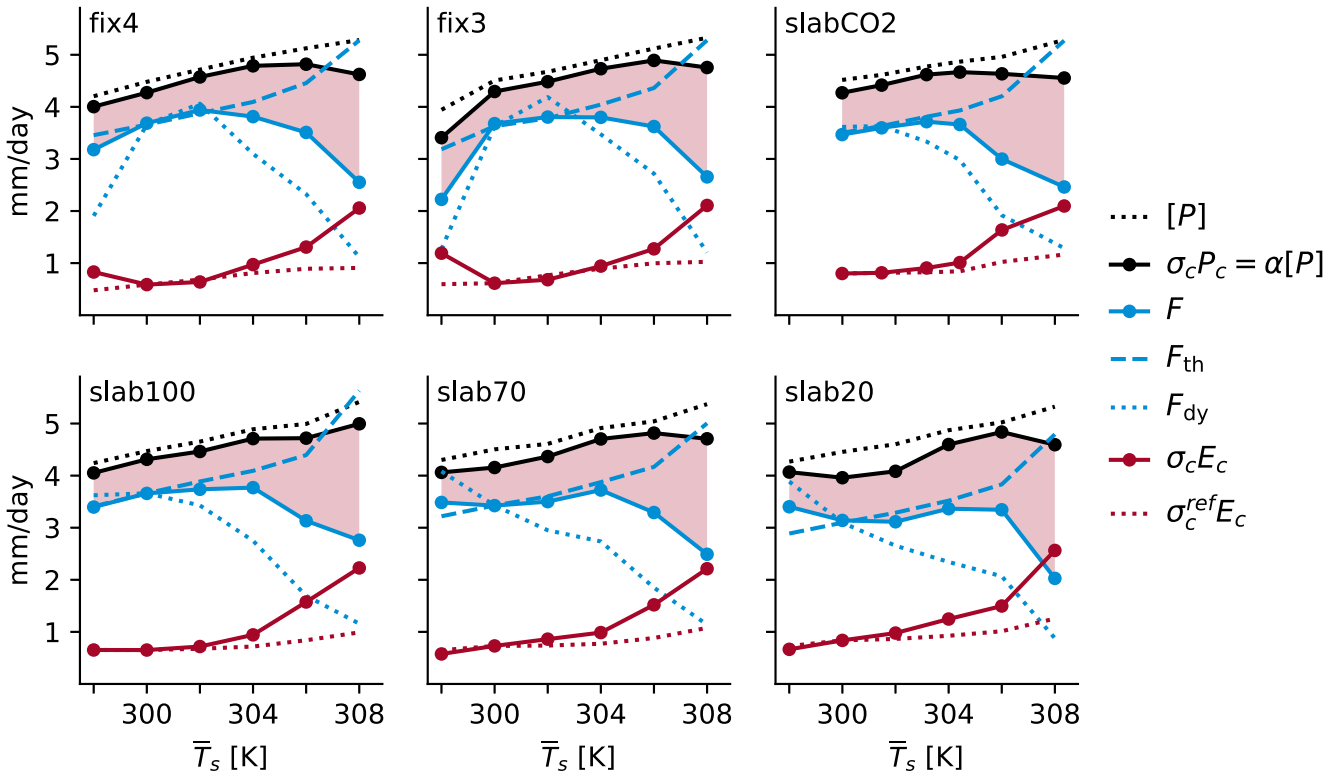

Figure 2. Changes in the moisture budget with warming. Each term in Equations 6 and 8 is shown. The solid red line shows local ascent-region evaporation $\sigma_c E_c$, which is also shown by the red-shaded area. The dotted red line shows $\sigma_c E_c$ if σ_c were fixed at its reference (300 K) value. The dashed and dotted blue lines show F_{th} and F_{dy}, which are the values that F would have if only thermodynamic or dynamic changes in moisture transport, respectively, were permitted (Section 3.3).

where square brackets denote the spatiotemporal average across the entire domain and $\alpha \approx 0.95$ is the fraction of total precipitation falling within the ascent region. Combining Equations 4 and 5 yields

$$\sigma_c E_c = \alpha[P] - F \tag{6}$$

where the AMT term

$$F \equiv \frac{\langle \overline{uq} \rangle_{\text{edge}}}{L_x} \tag{7}$$

is the water vapor flux into the ascent region normalized by domain length. Since α is near unity, we make the approximation

$$\sigma_c E_c \approx [P] - F. \tag{8}$$

Equation 8 says that local evaporation within the ascent region must account for the difference between domain-mean precipitation and the net flux of moisture into the ascent region.

Figure 2 shows how the terms of the moisture budget vary with $\overline{T}_s$. The increase in $[P]$ with warming—that is, the hydrological sensitivity—must balance increases in the net radiative cooling and sensible heating of the atmosphere (Pendergrass & Hartmann, 2014). Here, the hydrological sensitivity is between 1.8%/K and 2.8%/K depending on boundary configuration, in line with expectations from previous work (e.g., Held & Soden, 2006). Changes in $\sigma_c P_c$ are similar, departing from $[P]$ due to small variations in α. However, changes in the transport term F generally do not keep pace with the hydrological sensitivity. Instead, F initially increases or remains steady with warming before decreasing at higher temperatures. Even when F does increase with warming, it does

25766044, 2026, 1, Downloaded from https://agupubs.onlinelibrary.wiley.com/doi/10.1029/2025AV002040 by Adam, B Sokol - University Of Washington Lib , Wiley Online Library on [20/02/2026]. See the Terms and Conditions (https://onlinelibrary.wiley.com/terms-and-conditions) on Wiley Online Library for rules of use; OA articles are governed by the applicable Creative Commons License

2576604x, 2026, 1, Downloaded from https://agupubs.onlinelibrary.wiley.com/doi/10.1029/2025AV002040 by Adam, B Sokol - University Of Washington Lib , Wiley Online Library on [20/02/2026]. See the Terms and Conditions (https://onlinelibrary.wiley.com/terms-and-conditions) on Wiley Online Library for rules of use; OA articles are governed by the applicable Creative Commons License

so at a slower rate than precipitation, again with the exception of the first $\overline{T}_s$ increment in the fixed-T_s runs. Because AMT changes more slowly than precipitation, the difference between the two (shown by the red line and shading in Figure 2) increases by 10%/K–15%/K on average, although the rate of increase varies significantly with $\overline{T}_s$. In other words, as the surface warms, the circulation does not supply the ascent region with the additional moisture necessary to meet the growing precipitation demand, and the fraction of precipitation sourced from AMT decreases (Figure S4c in Supporting Information S1).

As a consequence of Equation 8, the growing gap between precipitation and AMT must be balanced by an increase in local evaporation within the ascent region, $\sigma_c E_c$. This can occur via increases in E_c and/or σ_c. While the *domain*-mean evaporation rate is constrained by the hydrological sensitivity, the same does not apply to the *ascent-region* mean, E_c. In the fixed-T_s simulations, E_c obeys approximate Clausius-Clapeyron scaling with a mean increase of 6%/K–7%/K (Figure S4b in Supporting Information S1). In the slab runs, the increase is slower at first, exhibiting sub-Clausius-Clapeyron sensitivity even with respect to the local T_s in the ascent region, which warms more slowly than $\overline{T}_s$. However, in the warmer simulations, increases in E_c approach and even exceed the Clausius-Clapeyron rate. Regardless, in all but a few simulations, E_c outpaces the hydrological sensitivity, meaning that increases in domain-mean evaporation come preferentially from the ascent region. Nevertheless, the increase in E_c is smaller than the 10%/K–15%/K increase in $[P] - F$, meaning changes in E_c alone are not sufficient to offset the growing moisture deficit in the ascent region (dotted red line in Figure 2). As a result, σ_c must increase.

3.3. Thermodynamic and Dynamic Influences on Moisture Transport

The previous section showed that changes in moisture transport do not keep up with the precipitation response to warming. As discussed in Section 1, a central component of the wet-gets-wetter and upped-ante mechanisms is the dominance of thermodynamically driven changes in AMT over compensating dynamically driven changes. In contrast, this section shows that the two components are similar in magnitude in our simulations, resulting in the slow response of total AMT to warming.

To separate the thermodynamic and dynamic components, we write the AMT term F in terms of the mean moisture flux convergence within the ascent region, then apply the Reynolds decomposition:

$$\begin{aligned} F &= -\sigma_c \langle \nabla \cdot \overline{u q} \rangle_c \\ &= -\sigma_c \left(\langle \overline{q} \nabla \cdot \overline{u} \rangle_c + \langle \overline{u} \cdot \nabla \overline{q} \rangle_c + \langle \nabla \cdot \overline{u' q'} \rangle_c \right). \end{aligned} \tag{9}$$

We can make three simplifications to Equation 9 due to the fact that horizontal gradients in $\overline{q}$ within the ascent region are small compared to those in $\overline{u}$. First, we approximate the first term on the right-hand side $\langle \overline{q} \nabla \cdot \overline{u} \rangle_c \approx -\langle q_c C_c \rangle$, where $C_c = -(\nabla \cdot \overline{u})_c$ is the mean convergence profile in the ascent region. We then neglect the second term, which is 1–2 orders of magnitude smaller than the first. Lastly, we neglect the third and final term, which represents eddy moisture flux convergence and accounts for only ∼2% of the total in our simulations. With these simplifications, we have

$$F \approx \sigma_c \langle q_c C_c \rangle, \tag{10}$$

which is accurate to within ∼5% (Figure S5 in Supporting Information S1). The benefit of Equation 10 is that F is expressed solely in terms of the mean convergence and specific humidity profiles in the ascent region, scaled by σ_c. This allows us to approximate what F would be at each $\overline{T}_s$ if only thermodynamic or dynamic changes were permitted:

$$F_{\text{th}} = \sigma_c^{\text{ref}} \langle q_c C_c^{\text{ref}} \rangle \tag{11}$$

$$F_{\text{dy}} = \sigma_c^{\text{ref}} \langle q_c^{\text{ref}} C_c \rangle \tag{12}$$

where ref denotes values from a reference climate, which we define as $\overline{T}_s = 300$ K. Changes in F_{dy} represent dynamically driven changes in AMT, that is, how AMT would respond to warming if the circulation was free to

2576604x, 2026, 1, Downloaded from https://agupubs.onlinelibrary.wiley.com/doi/10.1029/2025AV002040 by Adam, B Sokol - University Of Washington Lib , Wiley Online Library on [20/02/2026]. See the Terms and Conditions (https://onlinelibrary.wiley.com/terms-and-conditions) on Wiley Online Library for rules of use; OA articles are governed by the applicable Creative Commons License

change but the moisture field were fixed to its reference state. F_{th} represents thermodynamically driven changes in AMT, for which moisture can vary but the circulation is held fixed. It should be noted that F_{th} is not entirely free from dynamic influence, since model-simulated changes in the moisture field can be affected by circulation adjustments. Furthermore, we note that both F_{th} and F_{dy} assume fixed ascent fraction; we explored an alternative formulation of Equations 11 and 12 in which σ_c does not appear, but the conceptual interpretation is more convoluted.

Figure 2 shows that F_{th} (dashed blue line) increases monotonically with $\overline{T}_s$ at a rate similar to or exceeding $[P]$. This means that if the circulation were fixed, AMT alone could fuel the increase in precipitation needed to balance changes in atmospheric radiative cooling and sensible heating, and no increase in local evaporation ($\sigma_c E_c$) would be required to maintain moisture balance in the ascent region. In contrast, F_{dy} decreases markedly with warming (Figure 2, dotted blue line), with the exception of increases in the fixed-T_s runs associated with the merging of two convective zones. The trends in F_{th} and F_{dy} are similar in magnitude, indicating that dynamically driven changes in AMT cannot be neglected. Indeed, the simulated F falls between F_{th} and F_{dy}, reflecting substantial compensation between the two. The failure of AMT to scale with $[P]$ is entirely due to the large, negative dynamic response—that is, weakening of the circulation offsets Clausius-Clapeyron-driven increases in AMT.

3.4. Drivers of Circulation Change

The previous section showed that circulation weakening offsets thermodynamically driven increases in moisture transport. In this section we show that this weakening results from changes in circulation structure and the vertical profile of MSE. We quantify circulation strength as $-\omega_c^* = -\langle\omega_c\rangle/(p_s - p_t)$, which is the vertically averaged vertical velocity in the ascent-region troposphere. Figure 3a shows that, in the fixed-T_s simulations, the circulation at first strengthens with warming then weakens rapidly, mirroring the non-monotonic σ_c trend (Figure 1). In the slab simulations, the circulation weakens monotonically at an average rate of ∼12%/K. This is in line with the rate of Walker weakening in both coupled and atmosphere-only GCMs (Duffy & O'Gorman, 2023), and significantly outpaces the average GCM-predicted weakening of the zonal- and annual-mean Hadley circulation, which is ∼1%/K (Byrne et al., 2018; Lu et al., 2007). In the sensitivity tests with a 3D domain, the trends are qualitatively similar albeit noisier (Figure S2 in Supporting Information S1).

To understand the circulation response, we begin with the equilibrium, tropospheric MSE budget of the ascent region:

$$\langle\nabla\cdot(\overline{u}\overline{h})\rangle_c = Q_c. \tag{13}$$

Here, $h = c_pT + Lq + gz$ is the MSE, where c_p is the isobaric heat capacity of dry air and L the latent heat of vapourization. Other variables have their usual meanings. $Q = \langle R\rangle + H_L + H_S - \langle\nabla\cdot(\overline{u'h'})\rangle$ is the total MSE source due to diabatic and eddy processes, where R is the radiative flux divergence and $\nabla\cdot(\overline{u'h'})$ is the eddy MSE flux divergence. Individual MSE budget terms are shown in Figure S6 in Supporting Information S1.

Circulation strength and the MSE budget are connected via the gross moist stability (GMS), which can be thought of as the efficiency by which the mean circulation exports MSE from the ascent region. GMS has many definitions (Raymond et al., 2009); for our purposes, let

$$GMS = -g\frac{\langle\nabla\cdot(\overline{u}\overline{h})\rangle_c}{\omega_c^*} \tag{14}$$

such that positive GMS (J/kg) corresponds to a thermally direct circulation that exports MSE out of the ascent region. Note that this definition accounts for both horizontal and vertical advection of MSE. While many have defined GMS similarly (e.g., Inoue & Back, 2015; Raymond et al., 2009), others include only vertical advection (e.g., Byrne & Schneider, 2016; Wills et al., 2017). Combining Equations 13 and 14 yields

$$\omega_c^* = -g\frac{Q_c}{GMS}, \tag{15}$$

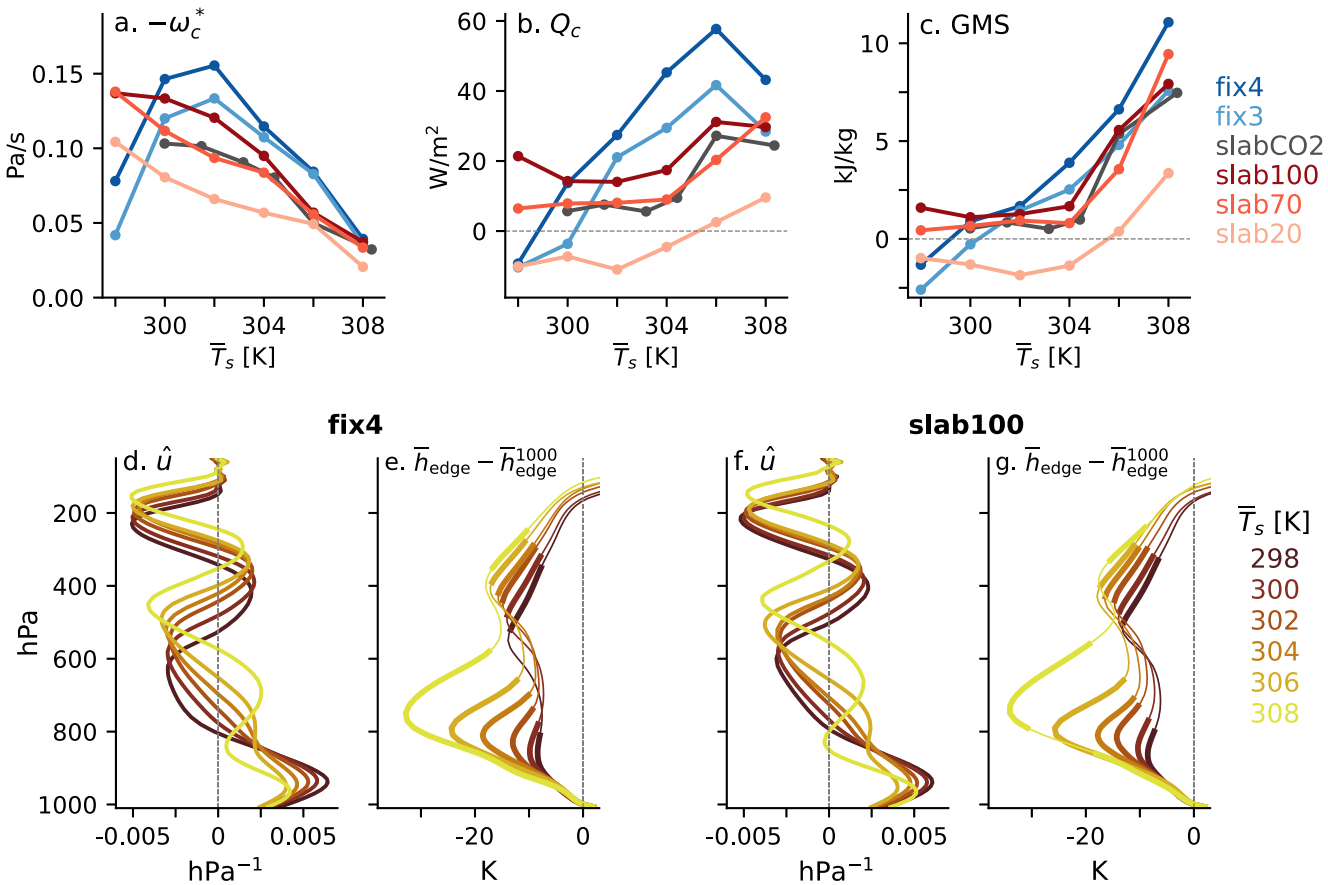

Figure 3. Drivers of circulation weakening. Trends in (a) circulation strength $-\omega^*$, (b) Q_c, and (c) GMS. (d, f) Normalized ascent-region inflow $\hat{u}$ (e, g) MSE profiles at the ascent-region boundary, h_{edge}, normalized by c_p and expressed as the deviation from its 1,000-hPa value. Lines are thicker at levels of mean inflow to the ascent region and thinner at levels of mean outflow.

from which we see that circulation weakening could be driven by decreases in total energy input and/or increases in GMS.

Figures 3b and 3c shows that both Q_c and GMS generally increase with warming, meaning they have compensating effects on circulation strength. The trend in Q_c is driven by increases in evaporation, which slightly outpace those in radiative cooling (Figure S6 in Supporting Information S1). In the fixed-T_s simulations, the trends in Q_c and GMS are approximately linear, with the exception of the Q_c decrease at the warmest $\overline{T}_s$. Between 298 and 302 K, as the two distinct regions of ascent merge, changes in Q_c outpace those in GMS, strengthening the circulation and giving rise to the non-monotonic trends noted in previous sections. In the slab simulations, trends in Q_c and GMS are weak between 300 and 304 K due to the weakening of T_s gradients with warming, which slows the increase in evaporation and horizontal MSE advection. Nevertheless, the fractional changes in GMS outpace those in Q_c, so the circulation weakens substantially.

To understand the GMS response to warming, we rewrite the ascent-region advective MSE tendency in terms of the column-integrated MSE flux at the region boundaries

$$-\langle \nabla \cdot (\overline{u}\overline{h}) \rangle_c = \frac{\langle \overline{u}\overline{h} \rangle_{edge}}{\sigma_c L_x}. \quad (16)$$

Motivated by Duffy and O'Gorman (2023), we define the normalized ascent-region inflow as

25766044, 2026, 1, Downloaded from https://agupubs.onlinelibrary.wiley.com/doi/10.1029/2025AV002040 by Adam, B Sokol - University Of Washington Lib , Wiley Online Library on [20/02/2026]. See the Terms and Conditions (https://onlinelibrary.wiley.com/terms-and-conditions) on Wiley Online Library for rules of use; OA articles are governed by the applicable Creative Commons License

$$\hat{u} = -\frac{\overline{u}_{\text{edge}}}{\omega_c^* \sigma_c L_x}, \tag{17}$$

where the term $\omega_c^* \sigma_c L_x$ scales with the total circulation mass transport. Unlike $\overline{u}_{\text{edge}}$, which is influenced by both the strength and vertical structure of the circulation, changes in $\hat{u}$ reflect changes in vertical structure only.

Through Equations 14, 16, and 17, GMS can be concisely expressed in terms of the inflow and MSE profiles at the ascent-region boundaries:

$$GMS = -g\langle \hat{u}\overline{h}_{\text{edge}} \rangle. \tag{18}$$

Profiles of $\hat{u}$ and $\overline{h}_{\text{edge}}$ are shown in Figures 3d–3g for the fix4 and slab100 simulations (see Figure S8 in Supporting Information S1 for the other simulations). To first order, $\overline{h}_{\text{edge}}$ exhibits a C shape that has long been known to characterize the tropical MSE profile (Riehl & Malkus, 1958). The C shape deepens in response to warming, consistent with previous work (Arnold et al., 2013; Chou et al., 2013; J. Zhang & Huang, 2023) and most evident between 600 and 800 hPa. Closer inspection reveals two local minima between the surface and tropopause with slightly elevated MSE in between; the elevated mid-level MSE is the signature of mid-tropospheric outflow from the ascent region, which is also evident in the $\hat{u}$ profiles. This indicates that the circulation has a double-cell structure, which is a known feature of cloud-resolving simulations with organized convection (Bretherton et al., 2006; Grabowski et al., 2000; Lutsko & Cronin, 2024; Sokol & Hartmann, 2022).

The increase in GMS with warming can be explained by changes in the structure of $\hat{u}$ in addition to the deepening C shape of the MSE profile. Consistent with the expected expansion of the troposphere in response to warming, there is an upward shift of the deep outflow layer centered at ∼200 hPa. But more significant changes in vertical structure occur at lower levels, where there is marked deepening of the near-surface inflow layer: over the 10-K $\overline{T}_s$ range, the top of the inflow layer shifts upward from ∼800 hPa to ∼570 hPa, which has important implications for GMS. Across the entire $\overline{T}_s$ range, the inflow layer encompasses both MSE-rich air from the moist boundary layer as well as MSE-poor, free-tropospheric air from immediately above the boundary layer. As the inflow layer expands upward, the free-tropospheric contribution increases and, due to the deepening C shape of the MSE profile, becomes increasingly deficient in MSE relative to the boundary layer. Together, these changes reduce the low-level MSE flux into the ascent region. This drives an increase in the net export of MSE from the ascent region for a given circulation strength, resulting in greater GMS.

The increase in GMS with warming has both thermodynamic and dynamic drivers originating from changes in MSE and $\hat{u}$, respectively. While increases in GMS with warming have been discussed in other work (Chou et al., 2013; Wills et al., 2017), to our knowledge none of the previously proposed mechanisms involve deepening of the convective inflow layer. This is because a large portion of previous work on GMS has used intermediate-complexity models in which the circulation adopts a "first baroclinic mode" structure with a single overturning cell, either by design or in response to assumptions of convective quasi-equilibrium (Chou et al., 2013; Chou & Neelin, 2004; Neelin & Zeng, 2000; Peters & Bretherton, 2005). Such a structure contains inflow extending from the surface to ∼500 hPa (see Figure 1b in Bretherton & Sobel, 2002). In contrast, the much shallower inflow layers in our low-$\overline{T}_s$ simulations leave plenty of room for deepening in response to warming. This difference arises from the double-cell circulation structure seen here, which allows the inflow layer to deepen as the lower circulation cell expands vertically (Figures 3d and 3f). These results point to uncertain but potentially consequential coupling between vertical circulation structure and spatial patterns of precipitation change, which we discuss further in Section 4.

We expect that previously proposed mechanisms of GMS increase—namely, the deepening of the troposphere—are also active in our simulations. We decomposed GMS into components associated with horizontal and vertical MSE advection and found that the total warming response is driven entirely by the horizontal component (Text S3, Figure S7 in Supporting Information S1). Because tropospheric deepening affects the vertical component, we conclude that it is not the main driver of GMS trends in our simulations and suspect that it is offset by other changes in circulation structure.

25776044, 2026, 1, Downloaded from https://agupubs.onlinelibrary.wiley.com/doi/10.1029/2025AV002040 by Adam, B Sokol - University Of Washington Lib , Wiley Online Library on [20/02/2026]. See the Terms and Conditions (https://onlinelibrary.wiley.com/terms-and-conditions) on Wiley Online Library for rules of use; OA articles are governed by the applicable Creative Commons License

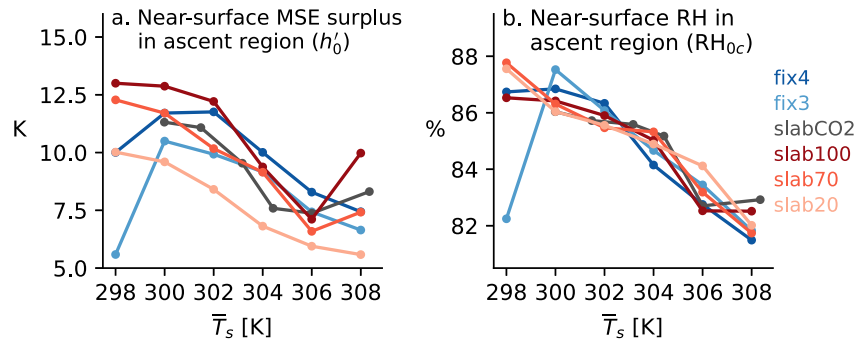

Figure 4. Near-surface thermodynamic change. (a) h_0', the anomalous near-surface MSE in the ascent region with respect to the domain mean (normalized by c_p). (b) Mean near-surface relative humidity in the ascent region.

3.5. Departure From Upped-Ante Expectations

The hydrological response to warming in our simulations contrasts sharply with the predictions of the upped-ante hypothesis. This result is surprising because the fixed-T_s experiments are, in many ways, the ideal test case for observing the seemingly straightforward thermodynamics underlying the upped-ante mechanism. Unlike our explanation of ascent-region expansion, the upped-ante mechanism deals primarily with the near-surface response to warming. In this section, we provide a near-surface perspective of the departure of our simulations from upped-ante expectations.

Synthesizing ideas from Neelin et al. (2003) and Y. Zhang and Fueglistaler (2019), the upped-ante mechanism relies on the fact that uniform warming should drive larger increases in near-surface MSE over warm T_s than over cool T_s, broadening the distribution of near-surface MSE. We first ask whether our simulations exhibit a similar pattern by examining the surplus of near-surface MSE in the ascent region relative to the domain average ($(h_0' = h_{0c} - [h_0])$). We denote near-surface variables with a 0 subscript and define them as the mass-weighted average between 950 hPa and the surface. In contrast to upped-ante expectations, Figure 4a shows that h_0' decreases substantially with warming, with some non-monotonicity reflecting the similar trends in σ_c and T_s gradients discussed previously. The full spatial patterns h_0 change shown in Figure S9 in Supporting Information S1 further confirm that MSE is *less* sensitive to warming over the warmest T_s than over the rest of the domain, resulting in a substantial narrowing of the near-surface MSE distribution with warming.

Having established that changes in near-surface MSE run counter to upped-ante expectations, we now consider the possible drivers of this surprising result. Changes in near-surface MSE can be driven by changes in boundary layer temperature and/or moisture content. In the fixed-T_s simulations, nonuniform changes in boundary layer temperature may occur despite uniform T_s change, due to nonuniform changes in the coupling between the surface and boundary layer. Such changes are modest in these simulations (not shown), and it is instead the moisture contribution that drives the surprising pattern of h_0 change. Figure 4b shows that near-surface relative humidity (RH_{0c}) in the ascent region decreases with warming by 0.5%/K–1.0%/K, whereas RH_0 in the subsiding part of the domain increases at a slightly faster rate (Figure S10 in Supporting Information S1). While numerically modest, these trends act to reduce gradients in RH_0 and therefore reduce h_0'. In the slab simulations, similar RH_0 trends are seen, but the temperature contribution is also important because warming is nonuniform. Weakening T_s gradients contribute to the rapid decrease in h_0' with warming up to 306 K, while strengthening T_s gradients cause a reversal of this trend between 306 and 308 K.

While a complete diagnosis of near-surface RH change is beyond our scope here, we suspect that the decrease in RH_{0c} with warming is driven by the circulation slowdown and associated reduction in AMT discussed in Section 3.2. The ability of large-scale circulation change to influence RH within regions of low-level convergence is supported by idealized GCM experiments (Natchiar et al., 2024) and a simple theoretical model of near-surface RH over oceans (Shakespeare & Roderick, 2024). The reduction in RH_{0c} can also be interpreted in light of the growing demand for local evaporation within the ascent region, as lower RH allows for a greater evaporation rate. This interpretation, too, ultimately ties back to circulation weakening, as it is the circulation-driven reduction in AMT that necessitates the increase in ascent-region evaporation (Section 3.2).

25766044, 2026, 1, Downloaded from https://agupubs.onlinelibrary.wiley.com/doi/10.1029/2025AV002040 by Adam, B Sokol - University Of Washington Lib , Wiley Online Library on [20/02/2026]. See the Terms and Conditions (https://onlinelibrary.wiley.com/terms-and-conditions) on Wiley Online Library for rules of use; OA articles are governed by the applicable Creative Commons License

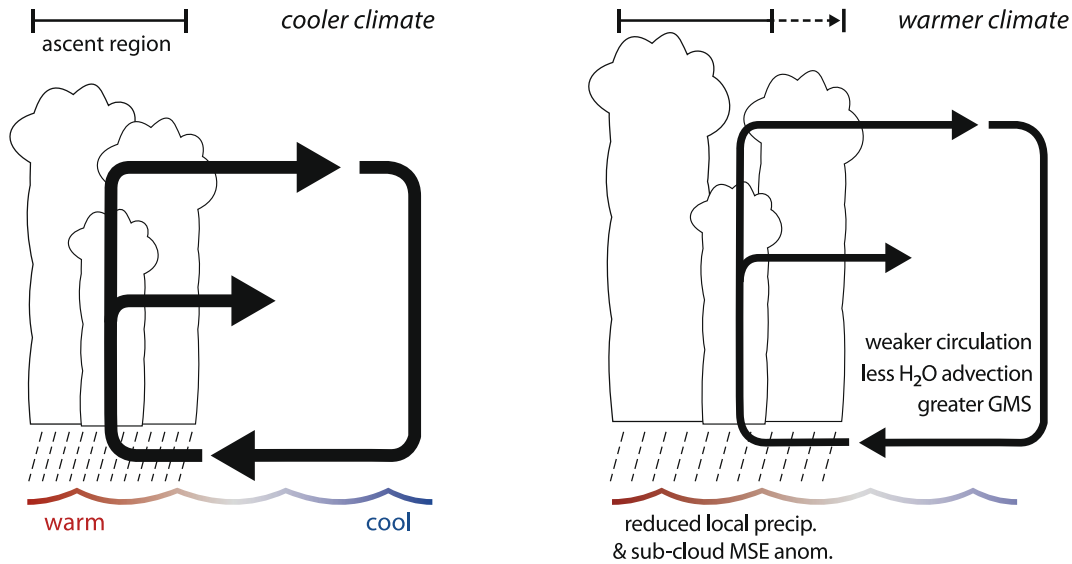

Figure 5. Schematic diagram of the mock-Walker response to warming discussed in this paper.

To conclude, we find that changes in near-surface thermodynamics depart from upped-ante expectations due to changes in near-surface RH. Through its influence on AMT, circulation weakening drives a reduction in ascent-region RH in a manner consistent with ascent region expansion. A broader takeaway from this section is that boundary-layer thermodynamics and T_s do not always change in lockstep; this point is emphasized by the notable differences in spatial structure between changes in T_s and the resulting changes in h_0 shown in Figure S9 in Supporting Information S1.

4. Discussion

We have presented a set of cloud-resolving, mock-Walker simulations in which surface warming drives an increase in ascent fraction and a wet-gets-*drier* precipitation response (Figure 5), in contrast to expectations set by the wet-gets-wetter and upped-ante paradigms of hydrological change. This result is particularly surprising considering our idealized experimental configuration, which one might prima facie expect to produce the anticipated narrowing of tropical ascent. The unexpected response is driven by rapid circulation weakening in response to warming, which reduces atmospheric moisture transport such that it cannot meet the moisture demand of increasing precipitation. To restore moisture balance, evaporation within the ascent region must increase. This occurs not only via increases in evaporation *rate*, but also via ascent region expansion, which allows moisture to be drawn from a larger surface area.

A central finding of this paper is that the vertical structure of the tropical circulation can have consequential impacts on large-scale patterns of precipitation change. The double-cell structure in our simulations differs markedly from the observed, single-cell structure of the real Walker circulation. Nevertheless, these results provide insight into possible mechanisms of change in regions where the overturning circulation deviates from the canonical first-baroclinic-mode structure, such as the Eastern Pacific (Back & Bretherton, 2006; Prange et al., 2024; C. Zhang et al., 2004, 2008). In several such regions, GCMs predict that seasonal convergence zones will widen in response to warming, in contrast to the expected narrowing of the zonal- and annual-mean ITCZ (Zhou et al., 2020). While our simulations are not intended to represent regional ITCZ dynamics, they suggest that regional differences in circulation structure may play a key role in shaping these divergent hydrological responses.

Our results also suggest that the accurate projection of hydrological change requires a detailed understanding of how vertical structure modulates circulation energetics in a warming climate. Changes in GMS in regions with complex ascent profiles may not be well explained by existing theories developed from models in which a single-cell structure is either prescribed or naturally dominant (Chou et al., 2013; Wills et al., 2017). While these theories still predict an increase in GMS with warming, even modest variations in vertical structure could impact the

25766044, 2026, 1, Downloaded from https://agupubs.onlinelibrary.wiley.com/doi/10.1029/2025AV002040 by Adam, B Sokol - University Of Washington Lib , Wiley Online Library on [20/02/2026]. See the Terms and Conditions (https://onlinelibrary.wiley.com/terms-and-conditions) on Wiley Online Library for rules of use; OA articles are governed by the applicable Creative Commons License

25776004x, 2026, 1, Downloaded from https://agupubs.onlinelibrary.wiley.com/doi/10.1029/2025AV002040 by Adam, B Sokol - University Of Washington Lib , Wiley Online Library on [20/02/2026]. See the Terms and Conditions (https://onlinelibrary.wiley.com/terms-and-conditions) on Wiley Online Library for rules of use; OA articles are governed by the applicable Creative Commons License

magnitude of the trend, with important implications for large-scale hydrological change. A timely opportunity for progress in this area is the second phase of the Radiative-Convective Equilibrium Model Intercomparison Project (RCEMIP-II, Wing et al., 2024), which commissioned mock-Walker warming experiments from multiple cloud-resolving models known to produce a wide variety of vertical circulation structures (Sokol & Hartmann, 2022). Here, we have laid the groundwork for understanding the relationship between hydrological change and the vertical structure of convection in such experiments.

Another significant result from these experiments is that near-surface thermodynamic changes are not necessarily a simple reflection of underlying T_s change. As shown in Section 3.5, changes in T_s and boundary-layer MSE differ significantly in their spatial structure due to changes in low-level RH. We suspect that these RH changes are dynamically driven in our simulations, as they are similar in structure to those in large-scale moisture convergence. However, near-surface humidity and, more broadly, boundary layer structure in numerical models are known to be sensitive to factors such as grid resolution, domain geometry, and the representation of subgrid-scale mixing (e.g., Honnert et al., 2011; Jeevanjee & Romps, 2013; Jenney et al., 2023; Sullivan & Patton, 2011). While the boundary-layer MSE changes in our simulations are consistent with ascent-region expansion, a complete understanding of low-level RH change requires a more targeted approach.

There are several caveats when it comes to the applicability of our results to the real Pacific Walker circulation. First, as noted above, is the difference in circulation structure between our simulations and the observed Walker circulation. Despite this, the rate of circulation weakening seen here is on par with GCM simulations that exhibit a single-cell structure (Duffy & O'Gorman, 2023). This suggests that while the mechanism of circulation slowdown in our runs may be more applicable to other tropical regions than to the Walker circulation, the resulting balance between dynamic and thermodynamic changes in moisture transport might still be representative of Walker response to warming. Second, our simulations lack ocean dynamics, which in the equatorial Pacific are tightly coupled to the Walker circulation (Bjerknes, 1969). Ocean dynamical mechanisms are thought to influence the Walker response to warming via their impact on zonal sea surface temperature gradients, but their role in the equilibrium response remains uncertain (Clement et al., 1996; Heede et al., 2020). While we have neglected ocean dynamics entirely, the slab simulations exhibit an overall weakening of T_s gradients with warming. This weakening is qualitatively consistent with GCM predictions (Knutson & Manabe, 1995; Lee et al., 2022), although it must be noted that GCMs generally fail to reproduce the observed pattern of T_s change over recent decades (Seager et al., 2022). The role of ocean dynamics in future Walker circulation weakening remains a critically important research area.

With the above caveats in mind, these results nevertheless present a physically self-consistent counterexample to long-established ideas about tropical hydrological change. In doing so, they suggest that the diversity of possible circulation responses to warming may be greater than previously appreciated, with important implications for regional precipitation patterns in different climates. A more complete theory of hydrological change must account for the range of circulation structures observed in the tropics and their influence on zonally asymmetric hydrological change.

Conflict of Interest

The authors declare no conflicts of interest relevant to this study.

Data Availability Statement

Code and model output for this study are available from https://zenodo.org/records/18165551 (Sokol, 2026). The System for Atmospheric Modeling (SAM) is available from http://rossby.msrc.sunysb.edu/SAM.html.

Acknowledgments
We thank two anonymous reviewers for their helpful feedback, Andrew Williams and Dennis Hartmann for constructive conversations, and Peter Blossey for maintaining the version of SAM used here. Simulations were performed using computational resources provided by the Cooperative Institute for Modeling the Earth System. This work was funded by awards NA18OAR4320123 and NA23OAR4320198 from the National Oceanic and Atmospheric Administration, U.S. Department of Commerce. The statements, findings, conclusions, and recommendations are those of the authors and do not necessarily reflect the views of the National Oceanic and Atmospheric Administration or the U.S. Department of Commerce.

References

Ahmed, F., Neelin, J. D., Hill, S. A., Schiro, K. A., & Su, H. (2023). A process model for ITCZ narrowing under warming highlights clear-sky water vapor feedbacks and gross moist stability changes in AMIP models. *Journal of Climate*, *36*(15), 4913–4931. https://doi.org/10.1175/JCLI-D-22-0689.1

Arnold, N. P., Kuang, Z., & Tziperman, E. (2013). Enhanced MJO-like variability at high SST. *Journal of Climate*, *26*(3), 988–1001. https://doi.org/10.1175/JCLI-D-12-00272.1

Back, L. E., & Bretherton, C. S. (2006). Geographic variability in the export of moist static energy and vertical motion profiles in the tropical Pacific. *Geophysical Research Letters*, *33*(17), L17810. https://doi.org/10.1029/2006GL026672

Bjerknes, J. (1969). Atmospheric teleconnections from the equatorial Pacific. *Monthly Weather Review*, *97*(3), 163–172. https://doi.org/10.1175/1520-0493(1969)097⟨0163:ATFTEP⟩2.3.CO;2

Bretherton, C. S., Blossey, P. N., & Khairoutdinov, M. (2005). An energy-balance analysis of deep convective self-aggregation above uniform SST. *Journal of the Atmospheric Sciences*, *62*(12), 4273–4292. https://doi.org/10.1175/JAS3614.1

Bretherton, C. S., Blossey, P. N., & Peters, M. E. (2006). Interpretation of simple and cloud-resolving simulations of moist convection–radiation interaction with a mock-Walker circulation. *Theoretical and Computational Fluid Dynamics*, *20*(5), 421–442. https://doi.org/10.1007/s00162-006-0029-7

Bretherton, C. S., & Sobel, A. H. (2002). A simple model of a convectively coupled walker circulation using the weak temperature gradient approximation. *Journal of Climate*, *15*(20), 2907–2920. https://doi.org/10.1175/1520-0442(2002)015⟨2907:ASMOAC⟩2.0.CO;2

Byrne, M. P., Pendergrass, A. G., Rapp, A. D., & Wodzicki, K. R. (2018). Response of the intertropical convergence zone to climate change: Location, width, and strength. *Current Climate Change Reports*, *4*(4), 355–370. https://doi.org/10.1007/s40641-018-0110-5

Byrne, M. P., & Schneider, T. (2016). Energetic constraints on the width of the intertropical convergence zone. *Journal of Climate*, *29*(13), 4709–4721. https://doi.org/10.1175/JCLI-D-15-0767.1

Chadwick, R., Boutle, I., & Martin, G. (2013). Spatial patterns of precipitation change in CMIP5: Why the rich do not get richer in the tropics. *Journal of Climate*, *26*(11), 3803–3822. https://doi.org/10.1175/JCLI-D-12-00543.1

Chou, C., & Neelin, J. D. (2004). Mechanisms of global warming impacts on regional tropical precipitation. *Journal of Climate*, *17*(13), 2688–2701. https://doi.org/10.1175/1520-0442(2004)017⟨2688:MOGWIO⟩2.0.CO;2

Chou, C., Wu, T.-C., & Tan, P.-H. (2013). Changes in gross moist stability in the tropics under global warming. *Climate Dynamics*, *41*(9), 2481–2496. https://doi.org/10.1007/s00382-013-1703-2

Clement, A. C., Seager, R., Cane, M. A., & Zebiak, S. E. (1996). An ocean dynamical thermostat. *Journal of Climate*, *9*(9), 2190–2196. https://doi.org/10.1175/1520-0442(1996)009⟨2190:AODT⟩2.0.CO;2

Clough, S. A., Shephard, M. W., Mlawer, E. J., Delamere, J. S., Iacono, M. J., Cady-Pereira, K., et al. (2005). Atmospheric radiative transfer modeling: A summary of the AER codes. *Journal of Quantitative Spectroscopy and Radiative Transfer*, *91*(2), 233–244. https://doi.org/10.1016/j.jqsrt.2004.05.058

Duffy, M. L., & O'Gorman, P. A. (2023). Intermodel spread in walker circulation responses linked to spread in moist stability and radiation responses. *Journal of Geophysical Research: Atmospheres*, *128*(1), e2022JD037382. https://doi.org/10.1029/2022JD037382

Elbaum, E., Garfinkel, C. I., Adam, O., Morin, E., Rostkier-Edelstein, D., & Dayan, U. (2022). Uncertainty in projected changes in precipitation minus evaporation: Dominant role of dynamic circulation changes and weak role for thermodynamic changes. *Geophysical Research Letters*, *49*(12), e2022GL097725. https://doi.org/10.1029/2022GL097725

Grabowski, W. W., Yano, J.-I., & Moncrieff, M. W. (2000). Cloud resolving modeling of tropical circulations driven by large-scale SST gradients. *Journal of the Atmospheric Sciences*, *57*(13), 2022–2040. https://doi.org/10.1175/1520-0469(2000)057⟨2022:CRMOTC⟩2.0.CO;2

Heede, U. K., Fedorov, A. V., & Burls, N. J. (2020). Time scales and mechanisms for the tropical pacific response to global warming: A tug of war between the ocean thermostat and weaker walker. *Journal of Climate*, *33*(14), 6101–6118. https://doi.org/10.1175/JCLI-D-19-0690.1

Held, I. M., Hemler, R. S., & Ramaswamy, V. (1993). Radiative-convective equilibrium with explicit two-dimensional moist convection. *Journal of the Atmospheric Sciences*, *50*(23), 3909–3927. https://doi.org/10.1175/1520-0469(1993)050⟨3909:RCEWET⟩2.0.CO;2

Held, I. M., & Soden, B. J. (2006). Robust responses of the hydrological cycle to global warming. *Journal of Climate*, *19*(21), 5686–5699. https://doi.org/10.1175/JCLI3990.1

Honnert, R., Masson, V., & Couvreux, F. (2011). A diagnostic for evaluating the representation of turbulence in atmospheric models at the kilometric scale. *Journal of the Atmospheric Sciences*, *68*(12), 2113–3131. https://doi.org/10.1175/JAS-D-11-061.1

Inoue, K., & Back, L. E. (2015). Gross moist stability assessment during TOGA COARE: Various Interpretations of gross moist stability. *Journal of the Atmospheric Sciences*, *72*(11), 4148–4166. https://doi.org/10.1175/JAS-D-15-0092.1

Jeevanjee, N., & Romps, D. M. (2013). Convective self-aggregation, cold pools, and domain size. *Geophysical Research Letters*, *40*(5), 994–998. https://doi.org/10.1002/grl.50204

Jenney, A. M., Ferretti, S. L., & Pritchard, M. S. (2023). Vertical resolution impacts explicit simulation of deep convection. *Journal of Advances in Modeling Earth Systems*, *15*(10), e2022MS003444. https://doi.org/10.1029/2022MS003444

Khairoutdinov, M. F., & Randall, D. A. (2003). Cloud resolving modeling of the ARM summer 1997 IOP: Model formulation, results, uncertainties, and sensitivities. *Journal of the Atmospheric Sciences*, *60*(4), 607–625. https://doi.org/10.1175/1520-0469(2003)060⟨0607:CRMOTA⟩2.0.CO;2

Knutson, T. R., & Manabe, S. (1995). Time-mean response over the tropical Pacific to increased C02 in a coupled ocean-atmosphere model. *Journal of Climate*, *8*(9), 2181–2199. https://doi.org/10.1175/1520-0442(1995)008⟨2181:TMROTT⟩2.0.CO;2

Lau, W. K. M., & Kim, K.-M. (2015). Robust Hadley Circulation changes and increasing global dryness due to CO_2 warming from CMIP5 model projections. *Proceedings of the National Academy of Sciences*, *112*(12), 3630–3635. https://doi.org/10.1073/pnas.1418682112

Lau, W. K. M., & Tao, W. (2020). Precipitation–radiation–circulation feedback processes associated with structural changes of the ITCZ in a warming climate during 1980–2014: An observational portrayal. *Journal of Climate*, *33*(20), 8737–8749. https://doi.org/10.1175/JCLI-D-20-0068.1

Lee, S., L'Heureux, M., Wittenberg, A. T., Seager, R., O'Gorman, P. A., & Johnson, N. C. (2022). On the future zonal contrasts of equatorial Pacific climate: Perspectives from Observations, Simulations, and Theories. *npj Climate and Atmospheric Science*, *5*(1), 1–15. https://doi.org/10.1038/s41612-022-00301-2

Lu, J., Vecchi, G. A., & Reichler, T. (2007). Expansion of the Hadley cell under global warming. *Geophysical Research Letters*, *34*(6), L06805. https://doi.org/10.1029/2006GL028443

Lutsko, N. J., & Cronin, T. W. (2024). The transition to double-celled circulations in mock-walker simulations. *Geophysical Research Letters*, *51*(14), e2024GL108945. https://doi.org/10.1029/2024GL108945

Ma, J., Chadwick, R., Seo, K.-H., Dong, C., Huang, G., Foltz, G. R., & Jiang, J. H. (2018). Responses of the tropical atmospheric circulation to climate change and connection to the hydrological cycle. *Annual Review of Earth and Planetary Sciences*, *46*(1), 549–580. https://doi.org/10.1146/annurev-earth-082517-010102

Merlis, T. M., & Schneider, T. (2011). Changes in zonal surface temperature gradients and walker circulations in a wide range of climates. *Journal of Climate*, *24*(17), 4757–4768. https://doi.org/10.1175/2011JCLI4042.1

Mlawer, E. J., Taubman, S. J., Brown, P. D., Iacono, M. J., & Clough, S. A. (1997). Radiative transfer for inhomogeneous atmospheres: RRTM, a validated correlated-k model for the longwave. *Journal of Geophysical Research*, *102*(D14), 16663–16682. https://doi.org/10.1029/97JD00237

Natchiar, S. R. M., Webb, M. J., Lambert, F. H., Vallis, G. K., Morcrette, C. J., Holloway, C. E., et al. (2024). Reduction in the tropical high cloud fraction in response to an indirect weakening of the Hadley cell. *Journal of Advances in Modeling Earth Systems*, *16*(5), e2023MS003985. https://doi.org/10.1029/2023MS003985

25776004, 2026, 1, Downloaded from https://agupubs.onlinelibrary.wiley.com/doi/10.1029/2025AV002040 by Adam, B Sokol - University Of Washington Lib , Wiley Online Library on [20/02/2026]. See the Terms and Conditions (https://onlinelibrary.wiley.com/terms-and-conditions) on Wiley Online Library for rules of use; OA articles are governed by the applicable Creative Commons License

Neelin, J. D., Chou, C., & Su, H. (2003). Tropical drought regions in global warming and El Niño teleconnections. *Geophysical Research Letters*, *30*(24), 2275. https://doi.org/10.1029/2003GL018625

Neelin, J. D., & Zeng, N. (2000). A quasi-equilibrium tropical circulation model—Formulation. *Journal of the Atmospheric Sciences*, *57*(11), 1741–1766. https://doi.org/10.1175/1520-0469(2000)057<1741:aqetcm>2.0.co;2

Pendergrass, A. G., & Hartmann, D. L. (2014). The atmospheric energy constraint on global-mean precipitation change. *Journal of Climate*, *27*(2), 757–768. (Publisher: American Meteorological Society). https://doi.org/10.1175/JCLI-D-13-00163.1

Peters, M. E., & Bretherton, C. S. (2005). A simplified model of the walker circulation with an interactive ocean mixed layer and cloud-radiative feedbacks. *Journal of Climate*, *18*(20), 4216–4234. https://doi.org/10.1175/JCLI3534.1

Pierrehumbert, R. T. (1995). Thermostats, radiator fins, and the local runaway greenhouse. *Journal of the Atmospheric Sciences*, *52*(10), 1784–1806. https://doi.org/10.1175/1520-0469(1995)052⟨1784:TRFATL⟩2.0.CO;2

Prange, M., Stevens, B., & Buehler, S. A. (2024). Seasonal emergence and circulation coupling of moist layers over the tropical Atlantic. *Geophysical Research Letters*, *51*(15), e2024GL108865. https://doi.org/10.1029/2024GL108865

Raymond, D. J., Sessions, S. L., Sobel, A. H., & Fuchs (2009). The mechanics of gross moist stability. *Journal of Advances in Modeling Earth Systems*, *1*(3), 9. https://doi.org/10.3894/JAMES.2009.1.9

Riehl, H., & Malkus, J. S. (1958). On the heat balance in the equatorial trough zone. *Geophysica*, *6*, 503–537.

Schwendike, J., Berry, G. J., Reeder, M. J., Jakob, C., Govekar, P., & Wardle, R. (2015). Trends in the local Hadley and local Walker circulations. *Journal of Geophysical Research: Atmospheres*, *120*(15), 7599–7618. https://doi.org/10.1002/2014JD022652

Seager, R., Henderson, N., & Cane, M. (2022). Persistent discrepancies between observed and modeled trends in the tropical Pacific Ocean. *Journal of Climate*, *35*(14), 4571–4584. (Publisher: American Meteorological Society Section: Journal of Climate). https://doi.org/10.1175/JCLI-D-21-0648.1

Seager, R., Naik, N., & Vecchi, G. A. (2010). Thermodynamic and dynamic mechanisms for large-scale changes in the hydrological cycle in response to global warming. *Journal of Climate*, *23*(17), 4651–4668. https://doi.org/10.1175/2010JCLI3655.1

Shakespeare, C. J., & Roderick, M. L. (2024). What controls near-surface relative humidity over the ocean? *Journal of Advances in Modeling Earth Systems*, *16*(6), e2023MS004168. https://doi.org/10.1029/2023MS004168

Sokol, A. B. (2026). *Code and data for "No "wet gets wetter" in kilometer-scale mock-Walker circulations" by Sokol et al. (2026)*. Zenodo. https://doi.org/10.5281/zenodo.18165551

Sokol, A. B., & Hartmann, D. L. (2022). Congestus mode invigoration by convective aggregation in simulations of radiative-convective equilibrium. *Journal of Advances in Modeling Earth Systems*, *14*(7), e2022MS003045. https://doi.org/10.1029/2022MS003045

Su, H., Wu, L., Zhai, C., Jiang, J. H., Neelin, J. D., & Yung, Y. L. (2020). Observed tightening of tropical ascent in recent decades and linkage to regional precipitation changes. *Geophysical Research Letters*, *47*(3), e2019GL085809. https://doi.org/10.1029/2019GL085809

Sullivan, P. P., & Patton, E. G. (2011). The effect of mesh resolution on convective boundary layer statistics and structures generated by large-eddy simulation. *Journal of the Atmospheric Sciences*, *68*(10), 2395–2415. https://doi.org/10.1175/JAS-D-10-05010.1

Vecchi, G. A., & Soden, B. J. (2007). Global warming and the weakening of the tropical circulation. *Journal of Climate*, *20*(17), 4316–4340. https://doi.org/10.1175/JCLI4258.1

Wills, R. C., Levine, X. J., & Schneider, T. (2017). Local energetic constraints on walker circulation strength. *Journal of the Atmospheric Sciences*, *74*(6), 1907–1922. https://doi.org/10.1175/JAS-D-16-0219.1

Wing, A. A., Reed, K. A., Satoh, M., Stevens, B., Bony, S., & Ohno, T. (2018). Radiative–convective equilibrium model intercomparison project. *Geoscientific Model Development*, *11*(2), 793–813. https://doi.org/10.5194/gmd-11-793-2018

Wing, A. A., Silvers, L. G., & Reed, K. A. (2024). RCEMIP-II: Mock-Walker simulations as phase II of the radiative–convective equilibrium model intercomparison project. *Geoscientific Model Development*, *17*(16), 6195–6225. https://doi.org/10.5194/gmd-17-6195-2024

Wodzicki, K. R., & Rapp, A. D. (2016). Long-term characterization of the Pacific ITCZ using TRMM, GPCP, and ERA-Interim. *Journal of Geophysical Research: Atmospheres*, *121*(7), 3153–3170. https://doi.org/10.1002/2015JD024458

Zhang, C., McGauley, M., & Bond, N. A. (2004). Shallow meridional circulation in the tropical eastern Pacific. *Journal of Climate*, *17*(1), 133–139. https://doi.org/10.1175/1520-0442(2004)017⟨0133:SMCITT⟩2.0.CO;2

Zhang, C., Nolan, D. S., Thorncroft, C. D., & Nguyen, H. (2008). Shallow meridional circulations in the tropical atmosphere. *Journal of Climate*, *21*(14), 3453–3470. https://doi.org/10.1175/2007JCLI1870.1

Zhang, J., & Huang, P. (2023). Integrated changes in tropical precipitation and circulation under global warming: Moist static energy budget and the role of sea surface warming pattern. *Climate Dynamics*, *61*(11), 5687–5698. https://doi.org/10.1007/s00382-023-06877-6

Zhang, Y., & Fueglistaler, S. (2019). Mechanism for increasing tropical rainfall unevenness with global warming. *Geophysical Research Letters*, *46*(24), 14836–14843. https://doi.org/10.1029/2019GL086058

Zhou, W., Leung, L. R., Lu, J., Yang, D., & Song, F. (2020). Contrasting recent and future ITCZ changes from distinct tropical warming patterns. *Geophysical Research Letters*, *47*(22), e2020GL089846. https://doi.org/10.1029/2020GL089846

25776044, 2026, 1, Downloaded from https://agupubs.onlinelibrary.wiley.com/doi/10.1029/2025AV002040 by Adam, B Sokol - University Of Washington Lib , Wiley Online Library on [20/02/2026]. See the Terms and Conditions (https://onlinelibrary.wiley.com/terms-and-conditions) on Wiley Online Library for rules of use; OA articles are governed by the applicable Creative Commons License